Regular Article

PHYSICAL CHEMISTRY RESEARCH
Published by the
Iranian Chemical Society
www.physchemres.org
info@physchemres.org

Phys. Chem. Res., Vol. 13, No. 2, 401-412, June 2025
DOI: 10.22036/pcr.2025.491189.2600

Optical Absorption and High-Order Harmonic Generation Spectra of Uric Acid Crystal and Its Metabolites: A TDDFT Study

F. Mohammadtabar[a], R. Rajaie Khorasani[a], H. Mohammadi-Manesh[b,*] and A. Kazempour[c,d]

[a]*Department of Chemistry, NT.C., Islamic Azad University, Tehran, Iran*
[b]*Department of Chemistry, Faculty of Science, Yazd University, P.O. Box: 89195-741, Yazd, Iran*
[c]*Department of Physics, Payame Noor University, P.O. Box: 119395-3697, Tehran, Iran*
[d]*Nano Structured Coatings Institute of Yazd Payame Noor University, Yazd PO Code: 89431-74559, Iran*
(Received 28 November 2024, Accepted 24 May 2025)

Purine and pyrimidine bases are naturally produced in living organisms, and dietary nucleic acids are metabolized into waste products within the human body. Uric acid, the final product of purine metabolism, is associated with various diseases when present at elevated levels. In this study, we used time-dependent density functional theory to analyze the optical absorption and high-order harmonic generation spectra of the uric acid molecule and crystal, along with its repair metabolites, 5-hydroxyisourate and allantoin. Our results reveal distinct optical properties among these compounds, showcasing significant differences. Notably, variations in the energy excitation range, dipole strength function in the optical absorption cross-section spectra, as well as marked differences in the plateau region, cut-off harmonic, anisotropy, and harmonic yield in the high-order harmonic generation spectra, were observed. These findings indicate that the spectral features of uric acid and its derivatives could be valuable for detecting uric acid accumulation and for studying intermediate and final products of the uric acid repair process. Overall, high-order harmonic and optical absorption cross-section spectra emerge as promising tools for exploring disease-related metabolites, with potential applications in early detection and prevention of conditions linked to abnormal uric acid levels.

Keywords: Uric acid, Time-dependent density functional theory, Linear absorption spectrum, Higher-order harmonic generation, Octopus code

INTRODUCTION

Uric acid (UA) is the final product of purine nucleotide degradation in humans (Fig. 1) [1]. When the uric acid molecule accumulates, hydrogen bonding between UA molecules can lead to crystal formation, contributing to the development of gout disease [2-4]. Hyperuricemia is also associated with several other conditions, including fatty liver [5], primary hypertension [6], coronary heart disease [7], Parkinson's disease [8], and metabolic syndrome [9]. Unlike humans, birds, reptiles, and most primates possess the uricase enzyme, which catalyzes the oxidation of UA into allantoin, carbon dioxide, and hydrogen peroxide (Fig. 2). In humans, diseases caused by UA accumulation are often treated with drugs containing urate oxidase, a nonhuman proteolytic enzyme that oxidizes UA to allantoin [10-12]. The catalytic properties of urate oxidase have been extensively studied experimentally [13-15]. Research in molecular biology has shown that nearly all biological processes, whether structural or functional, static or dynamic, related to energy metabolism or information transfer, and physiology or pathology, are closely linked to hydrogen bonding [16]. Uric acid is a weak, hydrogenated organic acid [17]. Under normal physiological conditions (PH 7.4 and 37 °C), urate exists in plasma primarily in its mono-deprotonated ionic form and is observed as various salts formed from deprotonated or semi-deprotonated urate [18]. Monosodium urate (MSU) monohydrate, consisting of one urate molecule bonded to a sodium ion and a water molecule, leads to the formation of

*Corresponding author. E-mail: mohammadimanesh@yazd.ac.ir

gouty arthritis deposits. The morphology of MSU in the body consists of needle-like crystals that become lodged in tissues such as cartilage, causing inflammation. Rachael *et al.* investigated the properties of MSU crystals using Transmission Electron Microscopy (TEM) imaging along with SAED pattern analysis. They demonstrated that the needle-like structure and crystal stability result from hydrogen bonding between the purine rings. Furthermore, they suggested that the most effective method to prevent crystal growth is to disrupt these hydrogen bonds, as the hydrogen bonding within urate sheets is significantly weaker than the interaction between urate ions and Na^+ cations [19]. Zicheng and Chun Zhu examined the cluster structure between uric acid and water molecules using density functional theory (DFT) at the B3LYP-D3 (BJ)/6-31+G(d,p) level. Their study analyzed weak interactions as the planar monocluster configuration transitioned to a double-ring structure, employing atomic analysis (AIM) and reduced density gradient (RDG) methods. The results showed a red shift in the N-H peak in the theoretical Raman spectra of the uric acid molecule, indicating increased hydrogen interactions [20].

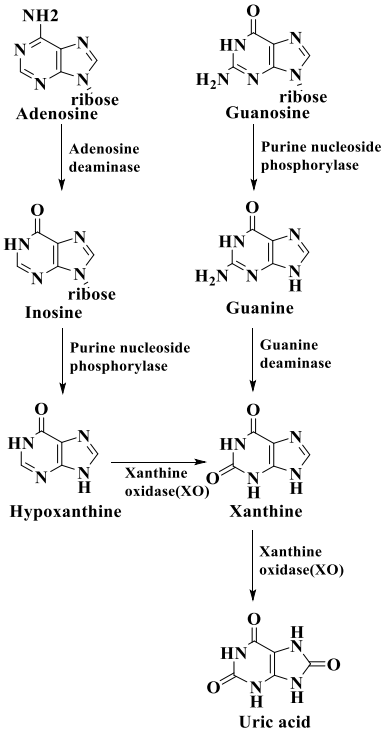

Fig. 1. Reactions of converting purines into uric acid.

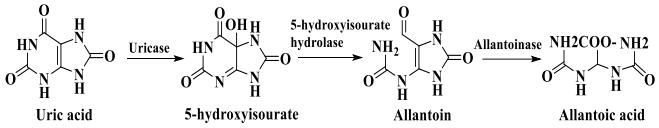

Fig. 2. The effect of uricase enzyme on uric acid.

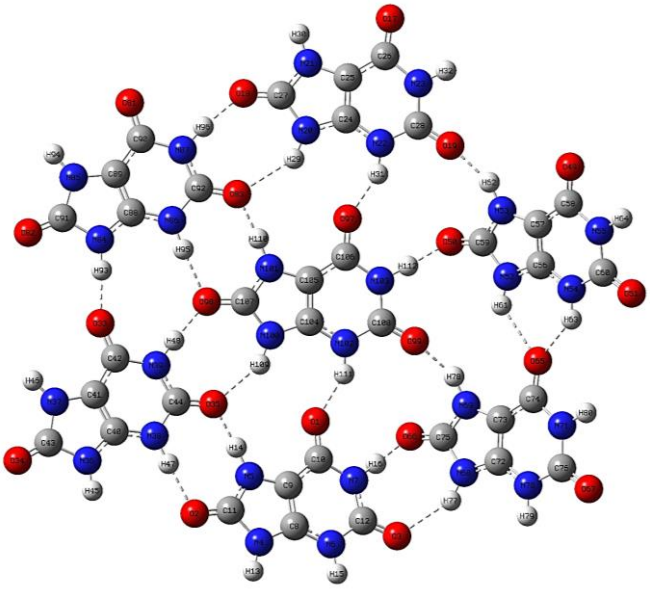

Fig. 3. The crystal structure of uric acid.

Kahn and Tipton investigated the theoretical mechanism of urate oxidase using stopped-flow absorbance and fluorescence spectrophotometry, and compared their findings with experimental data [14]. They identified two intermediates in the mechanism: 5-hydroxyisourate (a true product of urate oxidase) with an absorbance maximum at 302 nm, and allantoin (resulting from the natural hydrolysis of 5-hydroxyisourate in water) with an absorbance maximum at 240 nm. Altarsha et al. used various quantum methods, including semi-empirical ZINDO [21], HF-CIS [22], and time-dependent density functional theory (TDDFT) [23-26], to determine the UV spectra of uric acid, its monoanions, and dianions in the experimental range of 200-340 nm. They found that TDDFT closely reproduced the experimental data, demonstrating its reliability compared to other methods [27]. Norazmi *et al.* detected different concentrations of UA using Ultraviolet-Visible (UV-Vis) spectroscopy in the ultraviolet region. They defined the absorption cross-section of each uric acid concentration based on the Beer-Lambert law and showed that optical absorption peaks appear at constant

wavelengths across different concentrations, with varying peak intensities. This method was proposed for detecting different concentrations of UA and their absorption wavelengths [28]. With the advancement of computational power, complex calculations within the framework of TDDFT, such as calculation of optical absorption cross-section spectra and High-Order Harmonic Generation (HHG), have become feasible. These calculations enable the analysis of DNA bases, their derivatives (damaged forms), and their repair products [29]. Femtosecond and attosecond laser spectroscopy allow for the tracking of ultrafast dynamic processes in molecules [30-32]. When an atom, molecule, or surface is exposed to high-intensity laser radiation, electrons can absorb one or more photons and subsequently emit a single photon as they return to their initial state. This emitted photon has a frequency that is a multiple of the original laser frequency, a process known as HHG. HHG is described by a three-step semiclassical model [33-34]. Due to their high energy, emitted photons can serve as sources of coherent X-ray/XUV radiation or generate attosecond pulses. In a previous study, we explored the optical absorption cross-section and HHG spectra of thymine and its damaged forms, demonstrating their utility in identifying damaged DNA bases and derivatives. Our findings indicated that a laser with a cosinusoidal envelope and an intensity of 3.47×10^{14} W cm^{-2} provided superior results for identifying damaged forms compared to a Gaussian envelope at various intensities [30]. In this study, we employed TDDFT to calculate and compare the optical absorption cross-section and HHG spectra of uric acid, its crystal form, and the products of the uric acid repair process (5-hydroxyisourate and allantoin). The energy excitation ranges and peak intensities in the optical absorption cross-section spectra were found to be highly sensitive to the number of molecules, hydrogen bonding, and molecular structure. Similarly, key features of the HHG spectra, such as the plateau region, cut-off harmonic, anisotropy, harmonic yield, and constructive and destructive peak interferences, also showed strong dependence on these factors. The distinct spectral behaviors observed enable clear distinction between the uric acid crystal, the intermediate product (5-hydroxyisourate), and the final product (allantoin) formed during the uric acid repair process. The application of TDDFT to investigate the optical properties of uric acid and its metabolic derivatives in this study is entirely novel. Specifically, the HHG and optical absorption cross-section spectra presented have not been previously reported. By analyzing these spectra, distinct spectral signatures for each compound were identified. Uric acid, 5-hydroxyisourate, and allantoin are all derivatives of guanine and share structural similarities with it. Since the optical properties of these compounds have not been previously determined, the optical absorption cross-section spectra and transition energies of guanine have been included and compared with existing experimental data to validate the methodology. These findings pave the way for developing sensitive diagnostic tools to detect elevated uric acid levels, linked to various health issues, and provide insights into the uric acid repair process. The article is structured as follows: Section 2 outlines the methodology, Section 3 describes the computational details using the Octopus code, Section 4 presents the results, and Section 5 concludes the study.

COMPUTATIONAL METHODS

TDDFT is a powerful approach for solving the time-dependent Kohn-Sham equations. In this study, the Octopus code was used within the TDDFT framework to investigate time-dependent processes in both the linear (optical absorption cross-section) and nonlinear (HHG) regimes. Octopus uniquely operates without reliance on basis sets, solving the time-dependent Kohn-Sham equations in real-time by discretizing all quantities in real space [35-38]. Additionally, it employs norm-conserving pseudopotentials to describe the electron-ion interactions, significantly reducing computational demands [39-40]. The simulations start by solving the ground-state Kohn-Sham equations:

$$\widehat{H}_{\mathrm{KS}}\psi_i = E_i\psi_i \tag{1}$$

$$\left[-\frac{\nabla^2}{2} + \upsilon_{ext}(\mathbf{r}) + \upsilon_{\mathrm{Hartree}}(n;\mathbf{r}) + \upsilon_{\mathrm{xc}}(n;\mathbf{r})\right]\psi_i(\mathbf{r}) = E_i\psi_i(\mathbf{r}) \tag{2}$$

Where, υ_{ext} is the external potential, $\upsilon_{\mathrm{Hartree}}$ is the Hartree (or Coulomb energy) term and υ_{xc} represents the exchange-correlation energy term. The electron density, n, is expressed

$$n(\mathbf{r}) = \sum_{i=1}^{N} |\psi_i(\mathbf{r})|^2 \tag{3}$$

ψ_i represents the i-th ground-state wave function, and E_i denotes the corresponding ground-state energy.

Subsequently, the Kohn-Sham orbitals are propagated over time as:

$$\psi_i(t + \Delta t) = \exp\left(-i\hat{H}_{\mathrm{KS}}\Delta t\right)\psi_i(t) \quad (4)$$

It is important to note that only the occupied orbitals are propagated, eliminating the need to compute empty states. To calculate the linear optical absorption spectra, we employed the method proposed by Yabana and Bertsch [38]. In this approach, all system frequencies are excited by applying a small momentum (k) to the electrons, equivalent to imposing a perturbing electric field along the three Cartesian coordinates. This modifies the ground-state wave functions as follows:

$$\acute{}\psi_i = \exp(ik.r)\,\psi_i \quad (5)$$

These wave functions are then propagated for a specified time period, and the spectra are obtained from the dipole strength function, $S(\omega)$:

$$S(\omega) = -\frac{2\omega}{\pi}\mathrm{Im}[\alpha(\omega)] \quad (6)$$

Where the dynamic polarizability, $\alpha(\omega)$ is essentially the Fourier transform of the system's dipole moment, $d(t)$.

$$\alpha(\omega) = \frac{1}{k}\int \mathrm{d}t\mathrm{e}^{\mathrm{i}\omega t}[d(t) - d(0)] \quad (7)$$

To investigate the nonlinear optical properties, the system's evolution under the influence of a laser field is examined using the dipole approximation. The emitted harmonic spectra are calculated from the acceleration of the dipole moment [42].

$$H(\omega) \propto \left|\int \mathrm{d}t\mathrm{e}^{\mathrm{i}\omega t}\frac{\mathrm{d}^2}{\mathrm{d}t^2}d(t)\right|^2 \quad (8)$$

CALCULATION DETAILS

The calculations in this study were conducted using TDDFT using the Octopus code version 13.0. The local density approximation (LDA) with the Perdew-Zunger parameterization was employed for the exchange-correlation potential [35-43]. A real-space mesh comprising overlapping spheres with a radius of 3.0 Å centered on each nucleus and a grid spacing of 0.23 Å was utilized. For time propagation, a total propagation time of 15 fs was considered with a time step of 0.0032/eV, ensuring stability in the time-dependent propagation of the Kohn-Sham wave functions. To compute the optical absorption spectra, the perturbation electric field strength was set to 0.01/Å. For the HHG calculations, a laser pulse with a cosinusoidal envelope function and an intensity of 3.47×10^{14} W cm^{-2} was used. The selection of the laser intensity and envelope function was based on the authors' previous study, which demonstrated the feasibility of the chosen laser parameters [29]. To model the uric acid crystal, we considered seven uric acid molecules forming hydrogen bonds between the purine rings, constructing a segment of a urate sheet (Fig. 3). The urate sheet was generated using Avogadro 1.2.0 and GaussView 6.0.16, and the structure was then optimized using DFT with B3LYP/6-31++G(d,p) via Gaussian 09W. Visualization of the hydrogen bonds was performed using VMD 1.9.4a53 and Avogadro 1.2.0, with a distance/radius cut-off of 3.0 Å and an angle cut-off of 90°.

DISCUSSION AND RESULTS

Optical Absorption Cross-section Spectra

Figure 4 presents a comparison of the average optical absorption cross-section spectra of uric acid and its crystalline form. The corresponding excitation energies and dipole strength functions derived from the optical absorption spectra are summarized in Table 1. Additionally, the table includes excitation energies and the nature of the electronic transitions calculated through energy-domain computations using the Gaussian software. The first electronic transition for the uric acid crystal occurs at approximately 3.94 eV ($n\pi^*$), and the second transition appears around 4.52 eV ($n\pi^*$), exhibiting a lower dipole strength function compared to the first transition. For the uric acid molecule, the first and second electronic transitions are located at approximately 4.29 eV ($n\pi^*$) and 4.88 eV ($n\pi^*$), respectively, which are higher in energy compared to the crystal structure and display lower dipole strength functions. Overall, the comparison indicates that the excitation energies of the crystal structure occur at lower energy ranges with higher dipole strength function compared to the molecule, which can be attributed to molecular accumulation and hydrogen bonding within the

Table 1. Comparison of Excitation Energies, Electronic Transition Types, and Dipole Strength Functions of Uric Acid in Molecular and Crystalline Forms. (a) Values Derived from Optical Absorption Cross-section Spectra; (b) Values Computed Using Gaussian with the B3LYP/6-31++G(d,p) Basis Set

Uric acid molecule			Uric acid crystal		
E (eV)[a]	E (eV)[b]	S (1/eV)[a]	E (eV)[a]	E (eV)[b]	S (1/eV)[a]
4.29	4.54 $n\pi^*$	0.338	3.95	3.94 $n\pi^*$	2.632
4.88	4.59 $n\pi^*$	0.338	4.52	4.50 $n\pi^*$	2.523
5.93	5.54 $n\pi^*, n\sigma^*$	0.314	5.46	5.13 $n\pi^*$	2.089
6.36	6.06 $n\pi^*, n\sigma^*$	0.511	5.86	5.36 $n\pi^*$	4.079
6.72	6.07 $n\pi^*, n\sigma^*$	0.334	6.26	5.60 $n\pi^*$	4.767
7.28	6.17 $n\sigma^*$	1.611	6.67	5.80 $n\pi^*$	4.337

Table 2. Excitation Energies, Electronic Transition Types, and Dipole Strength Functions of the Guanine Base, along with Previous Experimental Data. (a) Values Derived from Optical Absorption Cross-section Spectra; (b) Values Computed Using Gaussian with the B3LYP/6-31++G(d,p) Basis Set; (c) Experimental Data Compiled in Reference [44]

E (eV)[a]	E (eV)[b]	S (1/eV)[a]	Exp[c]
4.14	4.55 $n\pi^*$	0.345	4.4-4.5
4.95	4.90 $n\pi^*$	0.412	4.9-5.0
5.54	5.55 $n\pi^*, \pi\pi^*$	0.051	5.7-5.8
5.90	5.90 $n\pi^*, \pi\pi^*$	1.733	6.1-6.3
6.30	5.91 $n\pi^*, \pi\pi^*, n\sigma^*$	0.706	6.6-6.7

crystal. As shown in Table 1, the most common electronic transitions in both the uric acid molecule and its crystalline form are $n\pi^*$ transitions, similar to those observed in guanine. The energy ranges of these electronic transitions, particularly in the uric acid molecule, also closely resemble those of guanine (Table 2). Since uric acid, 5-hydroxyisourate, and allantoin are guanine derivatives and, to the best of our knowledge, their optical absorption cross-section spectra have not been previously reported, Table 2 presents the corresponding results for guanine, compared with previously reported experimental excitation energies. Figure 5 compares the optical absorption cross-section spectra of guanine, uric acid, 5-hydroxyisourate, and allantoin molecules. Table 3 presents the excitation energies, electronic transition types, and dipole strength functions of the guanine derivatives (*i.e.*, uric acid, 5-hydroxyisourate, and allantoin), which closely resemble guanine in both structural and optical properties. The first and second electronic transitions of guanine occur at approximately 4.14 eV and 4.95 eV, respectively, showing good agreement

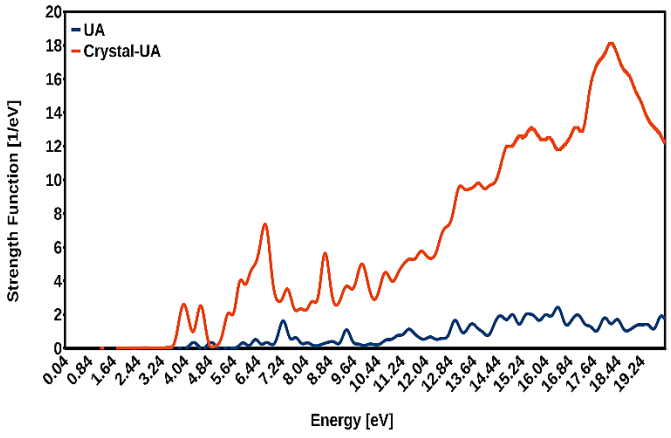

Fig. 4. Comparison of optical absorption cross-section spectra of the uric acid molecule and crystal form.

with experimental data [44]. The first electronic transition of the 5-hydroxyisourate molecule is observed around 4.84 eV ($n\pi^*$), which is at a higher energy than that of the uric acid molecule and exhibits a higher dipole strength function.

Subsequent transitions of 5-hydroxyisourate occur at even higher energy ranges compared to uric acid, although the dipole strength function decreases. The spectrum of allantoin exhibits the first and second electronic transitions at approximately 4.75 eV ($n\pi^*$) and 5.23 eV ($n\pi^*$), respectively, which are higher in energy than those of uric acid and display considerably lower dipole strength function. The subsequent transitions of allantoin also occur at higher energy ranges compared to both uric acid and 5-hydroxyisourate and are characterized by lower dipole strength function. The electronic transitions of uric acid, 5-hydroxyisourate, and allantoin are predominantly of the $n\pi^*$ type, similar to those observed in guanine. Additionally, the energy ranges of these transitions in uric acid, 5-hydroxyisourate, and allantoin closely resemble those of the guanine base. However, as mentioned earlier, the most distinguishing feature in the spectra of uric acid, compared to 5-hydroxyisourate and allantoin, is its notably lower energy range.

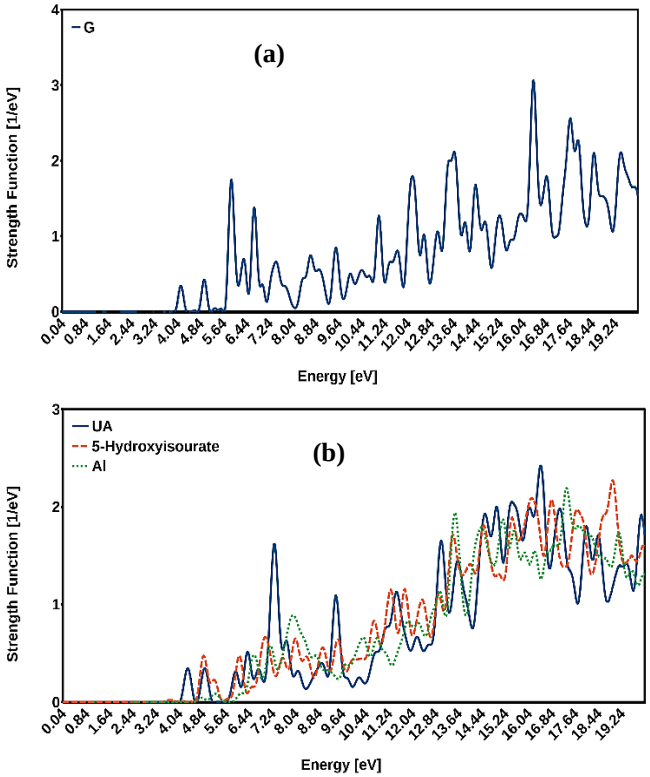

Fig. 5. Comparison of optical absorption cross-section spectra of (a) guanine and (b) uric acid, 5-hydroxyisourate, and allantoin molecules.

Table 3. Comparison of Excitation Energies, Electronic Transition Types, and Dipole Strength Functions of Uric Acid, 5-Hydroxyisourate, and Allantoin Molecules. (a) Values Derived from Optical Absorption Cross-section Spectra; (b) Values Computed Using Gaussian with the B3LYP/6-31++G(d,p) Basis Set

Uric acid			5-Hydroxyisoaurate			Allantoin		
E (eV)[a]	E (eV)[b]	S (1/eV)[a]	E (eV)[a]	E (eV)[b]	S (1/eV)[a]	E (eV)[a]	E (eV)[b]	S (1/eV)[a]
4.29	4.54 $n\pi^*$	0.338	4.84	4.56 $n\pi^*$	0.477	4.75	5.40 $n\pi^*$	0.047
4.88	4.59 $n\pi^*$	0.338	5.21	5.43 $n\pi^*$	0.225	5.23	5.94 $n\pi^*$	0.087
5.93	5.54 $n\pi^*$, $n\sigma^*$	0.314	6.07	5.72 $n\pi^*$	0.472	6.13	6.13 $n\pi^*$	0.088
6.36	6.06 $n\pi^*$, $n\sigma^*$	0.511	6.49	6.06 $n\pi^*$	0.156	6.56	6.54 $n\pi^*$, $n\sigma^*$	0.482
6.27	6.07 $n\pi^*$, $n\sigma^*$	0.334	6.94	6.09 $n\pi^*$	0.664	7.13	6.63 $n\pi^*$	0.571
7.28	6.17 $n\sigma^*$	1.611	7.54	6.16 $n\pi^*$	0.457	7.90	6.67 $n\pi^*$	0.897

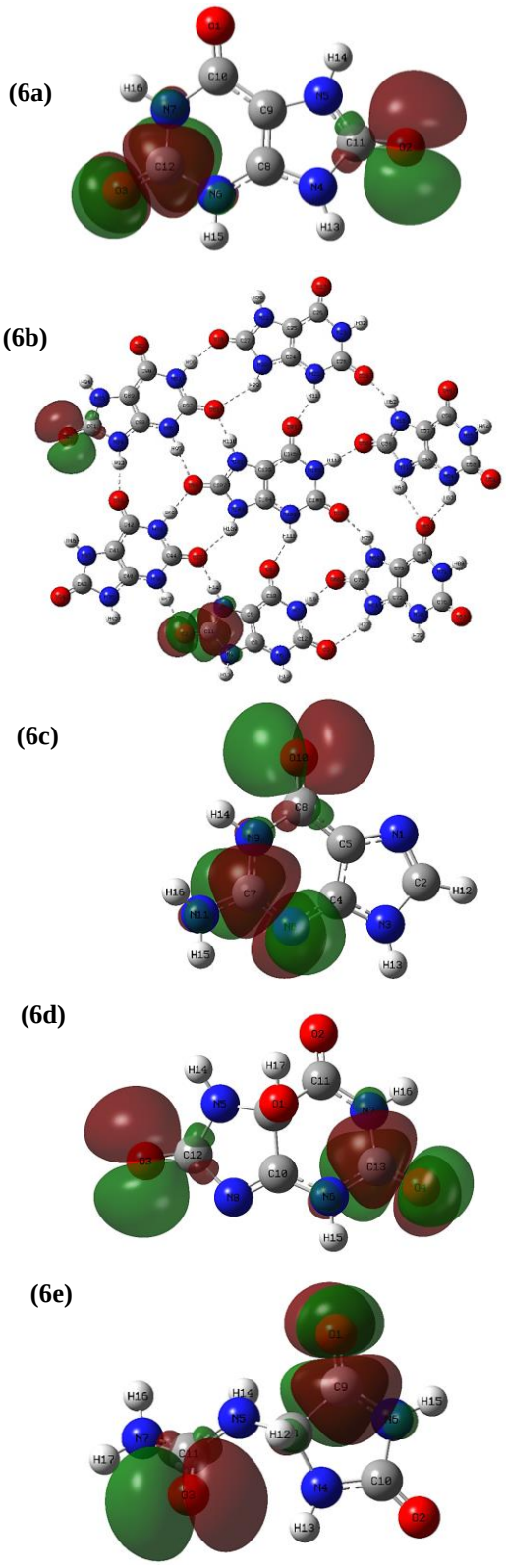

Fig. 6. HOMO-LUMO natural bond orbitals of (a) uric acid, (b) uric acid crystal, (c) guanine, (d) 5-hydroxyisourate, and (e) allantoin.

HHG Spectra

Uric acid crystal and uric acid molecule. Figure 7a presents the HHG spectra of the uric acid crystal in the x, y, and z directions, revealing significant anisotropy, particularly in the z direction, where harmonic intensities and the area under peaks are lower compared to the x and y directions. The x direction exhibits the highest harmonic yield, with strong initial odd harmonics followed by a broad plateau ending in a cut-off at 135. The y direction shows weaker initial peaks, with an increasing trend from the 5th to the 11th harmonic, followed by a plateau and cut-off similar to the x direction, but with diminished peak sharpness near the cut-off. In the z direction, the first three odd harmonics are intense and distinct, followed by a smaller plateau and an earlier cut-off at 55, where peaks are sharper than in other directions. Figure 7b displays the HHG spectra of the uric acid molecule, showing anisotropy in all three directions, especially the z direction, where peak intensities and area under peaks are lower. The x direction has the highest harmonic yield with intense initial odd harmonics, followed by an irregular increase, a plateau, and a cut-off at 76. The y direction shows lower initial harmonic intensities, an increase at the 7th harmonic, and a shorter plateau with an earlier cut-off at 55, where peak sharpness decreases. In the z direction, initial odd harmonics are less intense, followed by a peak indentation at the 7th harmonic, a small plateau, and an early cut-off at 27 with less resolved peaks. Significant differences are observed between the HHG spectra of crystalline and molecular uric acid in terms of intensity, anisotropy direction, cut-off harmonic range, and harmonic yield. Crystalline uric acid exhibits strong anisotropy in the z direction, while the single molecule shows anisotropy in all directions. Both structures yield the highest harmonics in the x direction, but with enhanced yield in the crystal. The crystal structure extends to higher-order cut-offs and has a broader plateau, with clearer initial odd harmonics in the x and z directions. The crystalline form shows sharper peaks overall and reduced destructive interference in initial harmonics, particularly in the z direction. These spectral distinctions reflect the accumulation of uric acid molecules and the formation of hydrogen bonds between them.

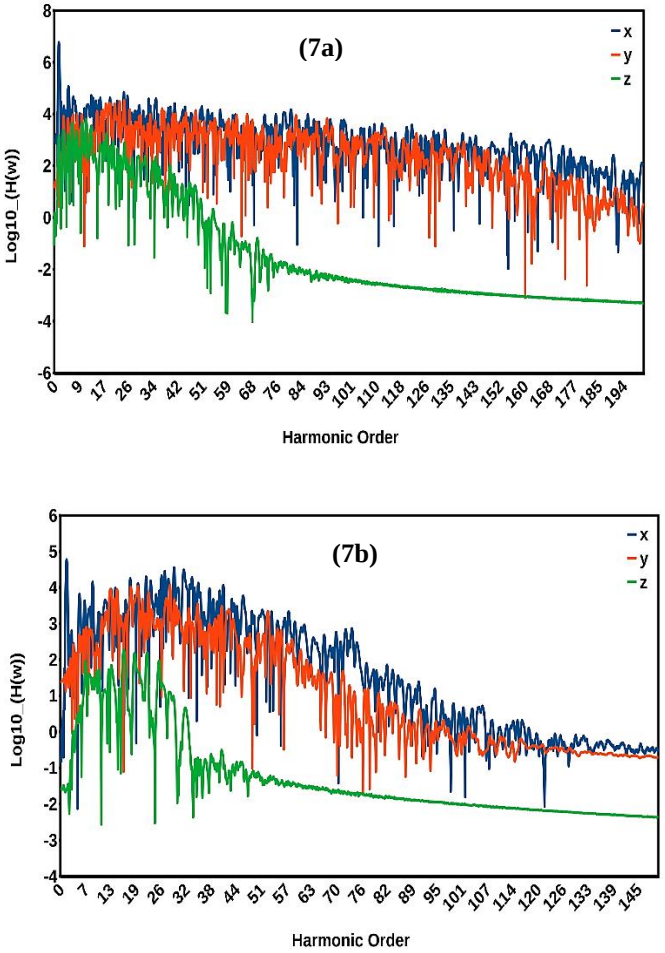

Fig. 7. HHG spectra of (a) uric acid crystal, (b) uric acid molecule.

5-Hydroxyisourate and Allantoin

Figure 8a shows the HHG spectra of 5-hydroxyisourate, which demonstrates anisotropy in all three directions, particularly at higher harmonic orders. The x direction has the highest harmonic yield, with intense and clear initial odd harmonic peaks. From the 7th to the 20th harmonics, peak intensity decreases, followed by an upward trend, a plateau region, and a cut-off harmonic around 75 (Table 4). In the y direction, initial peaks have very low or zero intensity and a peak indentation of -3, followed by a rise in intensity and a smaller plateau region, with a cut-off harmonic at 68. Peaks near the cut-off are less distinct than in the x direction. In the z direction, the peak structure differs significantly from the x and y directions, with a cut-off at 55 and reduced peak sharpness and separation, especially at higher orders. Figure 8b illustrates the HHG spectra of allantoin, displaying anisotropy mainly in the x direction, which also has the highest harmonic yield. Here, the initial harmonics are intense and distinct, with a decrease in peak intensity up to the 14th harmonic, followed by an increase, a plateau, and a cut-off harmonic at 95. Peaks around the cut-off show reduced intensity. In the y direction, initial peaks are weaker and less defined, with low-intensity peaks between the 5th and 9th harmonics, followed by a small plateau and a cut-off at 58, where peaks appear deformed. The z direction shows an even smaller plateau and an earlier cut-off at 47. The HHG spectra of uric acid, 5-hydroxyisourate, and allantoin exhibit notable differences in intensity, anisotropy direction, and cut-off harmonics. Notably, allantoin has a more extended plateau and later cut-off harmonic in the x direction at 95, compared to 75 for 5-hydroxyisourate. When comparing the HHG spectra of 5-hydroxyisourate and uric acid, uric acid exhibits greater anisotropy and lower peak intensity, area under the peaks, and peak separation in the z direction. The most significant difference in cut-off harmonics between these two molecules is also in the z direction, where 5-hydroxyisourate has a more coherent spectrum, a larger plateau, and a later cut-off. In the x direction, 5-hydroxyisourate shows more intense and distinct initial odd harmonics than uric acid. Comparing allantoin and uric acid reveals that uric acid has higher anisotropy in the z direction, while allantoin shows greater anisotropy in the x direction. Among uric acid, 5-hydroxyisourate, and allantoin, the most significant difference in anisotropy is observed for allantoin. This can be attributed to its structural distinction, as the six-membered ring has opened up in allantoin. Allantoin's cut-off harmonics occur later in all three directions, especially in the x and z directions, which show the greatest difference in plateau length and cut-off harmonics. Allantoin also has higher peak intensity, a larger area under peaks, better peak coherence, greater separation, and more prominent initial odd harmonics in the z direction.

Table 4. Comparison of Harmonic Cut-off and Anisotropy Direction of Uric Acid Crystal and Uric Acid, 5-Hydroxyisourate, and Allantoin Molecules

Structure	x	y	z	Anisotropy direction
Uric acid crystal	135	135	55	z
Uric acid	76	55	27	x, y, z
5-Hydroxyisourate	75	68	55	x, y, z
Allantoin	95	58	47	x

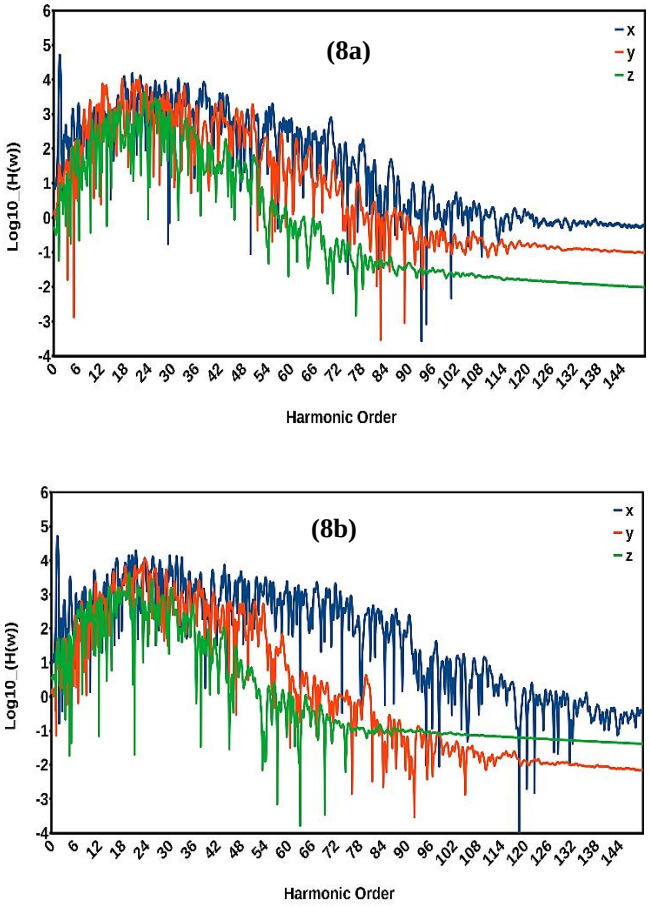

Fig. 8. HHG spectra of (a) 5-hydroxyisourate, (b) allantoin.

CONCLUSION

This study employed TDDFT to investigate the optical properties of uric acid, its crystal structure, and its repair products (5-hydroxyisourate and allantoin). For the first time, we calculated the optical absorption cross-section and HHG spectra of these compounds. Comparative analysis revealed significant differences in their optical absorption spectra, including variations in peak number, excitation energy range, and dipole strength function. The crystal structure exhibited more peaks, a lower excitation energy range, and an increased dipole strength function compared to the single molecule, likely due to molecular aggregation and hydrogen bonding. Among the repair products, 5-hydroxyisourate showed a higher excitation energy range with weaker electronic transitions, while allantoin demonstrated a lower excitation energy range and reduced dipole strength function, suggesting weaker electron transfers. The linear-response optical absorption cross-section spectra of uric acid, 5-hydroxyisoorotic acid, and allantoin (guanine base derivatives) agree with experimental guanine data. The HHG spectra provided additional insights: the uric acid crystal displayed distinct anisotropy, increased harmonic yield, and a larger cut-off region compared to the single molecule, highlighting its enhanced harmonic generation efficiency. Differences in intensity, anisotropy direction, and cut-off harmonic ranges were also observed in 5-hydroxyisourate and allantoin, with allantoin exhibiting the most pronounced variations. These findings highlight the unique optical and harmonic properties of each compound, suggesting that optical absorption and HHG spectra could serve as powerful tools for assessing uric acid and its metabolites. This approach has potential applications in the early detection and diagnosis of conditions associated with abnormal uric acid levels, as well as in the study of uric acid repair processes. Furthermore, it could aid in identifying compounds resulting from reactions with reactive oxygen and nitrogen species (ROS and RNS), reinforcing the role of uric acid in antioxidant defense [45]. In conclusion, this study demonstrates the utility of optical absorption and HHG

spectra for probing the structural and electronic properties of organic compounds, with promising applications in medical and biomedical fields.

REFERENCES

[1] Scheele, K. W., Examen Chemicum Calculi Urinarii. *Opuscula*. **1776**, *2*, 73-79, DOI: 10.1016/S0022-5347(17)36715-0.

[2] Lakshmi, D.; Whitcombe, M. J.; Davis, F.; Sharma, P. S.; Prasad, B. B., Electrochemical Detection of Uric Acid in Mixed and Clinical Samples: A Review. *Electroanalysis*. **2011**, *23*, 305-320, DOI: 10.1002/elan.201000525.

[3] Maiuolo, J.; Oppedisano, F.; Gratteri, S.; Muscoli, C.; Mollace, V., Regulation of Uric Acid Metabolism and Excretion. *Int. J. Cardiol.* **2016**, *213*, 8-14, DOI: 10.1016/j.ijcard.2015.08.109.

[4] Perez-Ruiz, F.; Dalbeth, N.; Bardin, T., A Review of Uric Acid, Crystal Deposition Disease, and Gout. *Adv. Ther.* **2015**, *32*, 31-41, DOI: 10.1007/s12325-014-0175-z.

[5] Liu, J.; Xu, C.; Ying, L.; Zang, S.; Zhuang, Z.; Lv, H.; Yang, W.; Luo, Y.; Ma, X.; Wang, L.; *et al*., Relationship of Serum Uric Acid Level with Non-Alcoholic Fatty Liver Disease and Its Inflammation Progression in Non-Obese Adults. *Hepatol. Res.* **2017**, *47*, E104-E112, DOI:10.1111/hepr.12734.

[6] Perticone, M.; Tripepi, G.; Maio, R.; Cimellaro, A.; Addesi, D.; Baggetta, R.; Sciacqua, A.; Sesti, G.; Perticone, F., Risk Reclassification Ability of Uric Acid for Cardiovascular Outcomes in Essential Hypertension. *Int. J. Cardiol.* **2017**, *243*, 473-478, DOI: 10.1016/j.ijcard.2017.05.051.

[7] Prasad, M.; Matteson, E. L.; Herrmann, J.; Gulati, R.; Rihal, C. S.; Lerman, L. O.; Lerman, A., Uric Acid is Associated with Inflammation, Coronary Microvascular Dysfunction, and Adverse Outcomes in Postmenopausal Women. *Hypertens* **2017**, *69*, 236-242, DOI: 10.1161/HYPERTENSIONAHA.116.08436.

[8] Pellecchia, M. T.; Savastano, R.; Moccia, M.; Picillo, M.; Siano, P.; Erro, R.; Vallelunga, A.; Amboni, M.; Vitale, C.; Santangelo, G.; Barone, P., Lower Serum Uric Acid Is Associated with Mild Cognitive Impairment in Early Parkinson's Disease: A 4-Year Follow-up Study. *J. Neural Transm.* **2016**, *123*, 1399-1402, DOI: 10.1007/s00702-016-1622-6.

[9] Kanbay, M.; Jensen, T.; Solak, Y.; Le, M.; Roncal-Jimenez, C.; Rivard, C.; Lanaspa, M. A.; Nakagawa, T.; Johnson, R. J., Uric Acid in Metabolic Syndrome: From an Innocent Bystander to a Central Player. *Eur. J. Intern. Med.* **2016**, *29*, 3-8, DOI: 10.1016/j.ejim.2015.11.026.

[10] Ronco, C.; Inguaggiato, P.; Bordoni, V.; De Cal, M.; Bonello, M.; Andrikos, E.; Assuman, Y.; Rattanarat, R.; Bellomo, R., Rasburicase therapy in acute hyperuricemia and renal dysfunction. *Contrib. Nephrol.* **2005**, *147*, 115-123, DOI: 10.1159/000082549.

[11] Cheson B. D.; Dutcher, B. S., Managing malignancy-associated hyperuricemia with rasburicase. *J. Support Oncol.* **2005**, *3*, 127-128, PMID: 15796443.

[12] Tsimberidou, A. M.; Keating, M. J., Hyperuricemic syndromes in cancer patients. *Contrib. Nephrol.* **2005**, *147*, 47-60, DOI: 10.1159/000182541.

[13] Kahn, K.; Serfozo, P.; Tipton, P. A., Identification of the True Product of the Urate Oxidase Reaction. *J. Am. Chem. Soc.* **1997**, *119*, 5435-5442, DOI: 10.1021/ja970375t.

[14] Kahn, K.; Tipton, P. A., Spectroscopic characterization of intermediates in the urate oxidase reaction. *Biochemistry.* **1998**, *37*, 11651-11659, DOI: 10.1021/bi980446g.

[15] 15-Imhoff, R. D.; Power, N. P.; Borrock, M. J.; Tipton, P. A., General Base Catalysis in the Urate Oxidase Reaction: Evidence for a Novel Thr-Lys Catalytic Diad. *Biochemistry.* **2003**, *42*, 4094-4100, DOI: 10.1021/bi027377x.

[16] Otto, R.; *et al*., Single solvent molecules can affect the dynamics of substitution reactions. *Nat. Chem.* **2012**, *4*, 534-538, DOI: 10.1038/nchem.1362.

[17] Burns, C. M.; WR. Disorders of purine and pyrimidine metabolism. In: Longo, F. A. D. L.; Kasper, D. L.; Hauser, S. L.; Jameson, J. L.; Loscalzo, J., editors. Harrison's principles of internal medicine. McGraw-Hill; New York, **2012**.

[18] Mandel, N. S.; Mandel, G. S., Monosodium urate monohydrate, the gout culprit. *J. Am. Chem. Soc.* **1976**, *98*(8), 2319-23, DOI: 10.1021/ja00424a054.

[19] Rachael, G. E.; Molloy; Weihao, Sun.; Jialu, Chen.; Wuzong, Zhou., Structure and cleavage of monosodium urate monohydrate crystals. *Chemical Communications.* 2019, *55*, 2178-2181, DOI: 10.1039/C8CC10050K.

[20] Zicheng, Cai.; Chun, Zhu.; Guoqing, Chen.; Yamin, Wu.; Jiao, Gu.; Chaoqun, Ma.; Hui, Gao.; Lei, Li.; Senqi, Guo., Study on intermolecular hydrogen bond of uric acid water-clusters. *Chemical Physics Letters*. **2023**, *818*, 140424, DOI: 10.1016/j.cplett.2023.140424.

[21] Zerner, M. C.; Ridely, J., An intermediate neglect of differential overlap technique for spectroscopy: Pyrrole and the azines. *Theor. Chim. Acta.* **1973**, *32*, 111-134, DOI: 10.1007/BF00528484.

[22] Foresman, J. B.; Head-Gordon, M.; Pople, J. A.; Frisch, M. J., Toward a systematic molecular orbital theory for excited states. *J. Phys. Chem.* **1992**, *96*, 135-149, DOI: 10.1021/j100180a030.

[23] Casida, M. E., Time-Dependent Density Functional Response Theory for Molecules in: Recent Advances in Density Functional Methods Vol. 1 (D. P. Chong, Ed.). World Scientic Singapore: **1995**, DOI: 10.1142/ 9789812830586_0005.

[24] Casida, M. E., Recent Developments and Application of Modern Density Functional Theory: Theoretical and Computational Chemistry in: J. M. Seminario (Ed.), Vol. 4, Elsevier, Amsterdam, **1996**.

[25] Casida, M. E.; Jamorski, C.; Casida, K. C.; Salahub, D. R., Imaginary Time Density Functional Calculation of Ground States of Atoms Using CWDVR Approach. *J. Chem. Phys.* **1998**, *108*, 4439-4449, DOI: 10.1063/ 1.475855.

[26] Jamorski, C.; Casida, M. E.; Salahub, D. R., Dynamic polarizabilities and excitation spectra from a molecular implementation of time-dependent density-functional response theory: N2 as a case study. *J. Chem. Phys.* **1996**, *104*, 5134-5147, DOI: 10.1063/1.471140.

[27] Altarsha, M.; Monard, G.; Castro, B., Quantum computations of the UV-visible spectra of uric acid and its anions. *Journal of Molecular Structure: THEOCHEM*. **2006**, *761*, 203-207, DOI: 10.1016/ j.theochem.2006.01.008.

[28] Norazmi, N.; Abdul Rasad, Z. R.; Mohamad, M.; Manap, H., Uric acid detection using UV-Vis spectrometer. *Materials Science and Engineering.* **2017**, *257*, 012031, DOI: 10.1088/1757899X/257/1/012031.

[29] Mohammadtabar, F.; Rajaie Khorasani, R.; Mohammadi-Manesh, H.; Kazempour, A., Study of optical absorption cross-section spectra and high-order harmonic generation of thymine, thymine glycol, and thymine dimer molecules. *Journal of Molecular Modeling*. **2022**, *28*, 402 DOI: 10.1007/s00894-022-05388-1.

[30] Baker, S.; Robinson, J. S.; Haworth, C. A.; Teng, H.; Smith, R. A.; Chirilaˇ, C. C.; Lein, M.; Tisch, J. W. G.; Marangos, J. P., Probing proton dynamics in molecules on an attosecond time scale. *Science.* **2006**, *312*, 424-427, DOI: 10.1126/science.1123904.

[31] Worner, H. J.; Bertrand, J. B.; Kartashov, D. V.; Corkum, P. B.; Villeneuve, D. M., Following a chemical reaction using high-harmonic interferometry. *Nature*. **2010**, *466*, 604-607, DOI: 10.1038/nature09185.

[32] Li, W.; Zhou, X.; Lock, R.; Patchkovskii, S.; Stolow, A.; Kapteyn, H. C.; Murnane, M. M., Time-resolved dynamics in N2O4 probed using high harmonic generation. *Science.* **2008**, *322*, 1207-1211, DOI: 10.1126/science.1163077.

[33] Corkum, P. B., Plasma perspective on strong field multiphoton ionization. *Phys. Rev. Lett.* **1993**, *71*, 1994-1997, DOI: 10.1103/PhysRevLett.71.1994.

[34] Krause, J. L.; Schafer, K. J.; Kulander, K. C., High-order harmonic generation from atoms and ions in the high intensity regime. *Phys. Rev. Lett.* **1992**, *68*, 3535-3538, DOI: 10.1103/PhysRevLett.68.3535.

[35] Beck, T. L., Real-space mesh techniques in density-functional theory. *Rev. Mod. Phys.* **2000**, *72*, 1041, DOI: 10.1103/RevModPhys.72.1041.

[36] Chelikowsky, J. R.; Troullier, N.; Saad, Y., Finite-difference-pseudopotential method: Electronic structure calculations without a basis. *Phys. Rev. Lett.* **1994**, *72*, 1240, DOI: 10.1103/PhysRevLett.72.1240. Vasiliev, I.; Ö˘güt, S.; Chelikowsky, J. R., Ab Initio Excitation Spectra and Collective Electronic Response in Atoms and Clusters. *Phys. Rev. Lett.* **1999**, *82* 1919, DOI: 10.1103/PhysRevLett.82.1919.

[37] Yabana, K.; Bertsch, G. F., Time-dependent local-density approximation in real time. *Phys. Rev.* **1996**, *54*, 4484, DOI: 10.1103/PhysRevB.54.4484.

[38] Iwata, J. I.; Yabana, K.; Bertsch, G. F., Real-space computation of dynamic hyperpolarizabilities. *J. Chem. Phys.* **2001**, *115*, 8773, DOI: 10.1063/1.1411996.

[39] Rubio, A.; Alonso, J. A.; Blase, X.; Balbás, L. C.; Louie, S. G., *Ab Initio* Photoabsorption Spectra and Structures of Small Semiconductor and Metal Clusters. *Phys. Rev. Lett.* **1996**, *77*, 247-250, DOI: 10.1103/ PhysRevLett.77.247.

[40] Schwerdtfeger, P., The pseudopotential approximation in electronic structure theory. *Chemphyschem.* **2011**, *12*, 3143-3155. DOI: 10.1002/ cphc.201100387.

[41] Pickett, W. E, Pseudopotential methods in condensed matter applications. *Comput. Phys. Rep.* **1989**, *9*, 115, DOI: 10.1016/ 0167-7977(89) 90002-6.

[42] Brabec, T.; Krausz, F., Intense few-cycle laser fields: Frontiers of nonlinear optics. *Rev. Mod. Phys.* **2000**, *72*, 545, DOI: 10.1103/RevModPhys.72.545.

[43] Kohn, W.; Sham, L. J., Self-consistent equations including exchange and correlation effects. *Phys Rev.* **1965**, *140*, 1133, DOI: 10.1103/PhysRev.140.A1133.

[44] Perdew, J. P.; Zunger, A., Self-interaction correction to densityfunctional approximations for many-electron systems. *Phys Rev B.* **1981**, *23*, 5048, DOI: 10.1103/PhysRevB.23.5048.

[45] Fulscher, M. P.; Serrano-Andres, L.; Roos, B., A Theoretical Study of the Electronic Spectra of Adenine and Guanine. *J. Am. Chem. Soc.* **1997**, *119*, 6168, DOI: https://doi.org/10.1021/ja964426i.

[46] Ames, B. N.; Cathcart, R.; Schwiers, E.; Hochstein, P., Uric Acid Provides an Antioxidant Defense in Humans against Oxidant- and Radical-Caused Aging and Cancer: A Hypothesis. *Proc. Natl. Acad. Sci.* **1981**, *78*, 6858-6862. DOI: 10.1073/pnas.78.11.6858.